Emergence of low-energy monopole strength in the neutron-rich calcium isotopes

J. Piekarewicz*
Department of Physics, Florida State University, Tallahassee, Florida 32306, USA
(Received 22 July 2017; revised manuscript received 29 August 2017; published 12 October 2017)

Background: The isoscalar monopole response of neutron-rich nuclei is sensitive to both the incompressibility coefficient of symmetric nuclear matter and the density dependence of the symmetry energy. For exotic nuclei with a large neutron excess, a low-energy component emerges that is driven by transitions into the continuum.
Purpose: While understanding the scaling of the giant monopole resonance with mass number is central to this work, the main goal of this paper is to explore the emergence, evolution, and origin of low-energy monopole strength along the even-even calcium isotopes: from ^{40}Ca to ^{60}Ca.
Methods: The distribution of isoscalar monopole strength is computed in a relativistic random phase approximation (RPA) using three effective interactions that have been calibrated to the properties of finite nuclei and neutron stars. A nonspectral approach is adopted that allows for an exact treatment of the continuum without any reliance on discretization. This is particularly critical in the case of weakly bound nuclei with single-particle orbits near the continuum. The discretization of the continuum is neither required nor admitted.
Results: For the stable calcium isotopes, no evidence of low-energy monopole strength is observed, even as the $1f^{7/2}$ neutron orbital is being filled and the neutron-skin thickness progressively grows. Further, in contrast to experimental findings, a mild softening of the monopole response with increasing mass number is predicted. Beyond ^{48}Ca, a significant amount of low-energy monopole strength emerges as soon as the weak-binding neutron orbitals ($2p$ and $1f^{5/2}$) become populated. The emergence and evolution of low-energy strength is identified with transitions from these weakly bound states into the continuum—which is treated exactly in the RPA approach. Moreover, given that models with a soft symmetry energy tend to reach the neutron-drip line earlier than their stiffer counterparts, an inverse correlation is identified between the neutron-skin thickness and the inverse energy weighted sum.
Conclusions: Despite experimental claims to the contrary, a mild softening of the giant monopole resonance is observed in going from ^{40}Ca to ^{48}Ca. Measurements for other stable calcium isotopes may be critical in elucidating the nature of the discrepancy. Moreover, given the early success in measuring the distribution of isoscalar monopole strength in the unstable ^{68}Ni nucleus, new measurements along the unstable neutron-rich calcium isotopes are advocated in order to explore the critical role of the continuum in the development of a soft monopole mode.

DOI: 10.1103/PhysRevC.96.044314

I. INTRODUCTION

What are the relatively few combinations of neutrons and protons that form a bound atomic nucleus is a question of critical importance to both nuclear structure and astrophysics [1,2]. Probing the limits of nuclear existence lies at the heart of the commissioning of state of the art rare isotope facilities throughout the world. However, mapping the precise boundaries of the nuclear landscape is enormously challenging. Given that the Coulomb interaction severely limits the number of neutrons that may be removed from a given isotope, the proton drip lines remains relatively close to the valley of stability. Indeed, the proton drip line has been determined experimentally up to protactinium, an isotope with atomic number $Z=91$. In stark contrast, the neutron drip line has been mapped only up to oxygen [3]. Thus, the neutron-rich landscape constitutes a fertile ground for research in nuclear structure and—due to its relevance to the r process and to the composition of the neutron-star crust—also in astrophysics [4].

Exceptional experimental advances have led to a paradigm shift in fundamental core concepts that have endured the test of time, such as the traditional nuclear magic numbers. Understanding the impact of such a paradigm shift in the development of novel modes of excitation in exotic nuclei has become a fruitful area of research [5]. Given the richness of these excitations, they offer a unique window into the nuclear dynamics that is often closed to other means [6]. In particular, the isovector dipole resonance has been shown to be highly sensitive to the equation of state of neutron-rich matter, specifically to the density dependence of the symmetry energy [7–10]. Indeed, measurements of the electric dipole polarizability in a variety of stable neutron-rich nuclei [11–14] and in the unstable ^{68}Ni isotope [15,16], provide an attractive alternative to parity-violating experiments to determine the neutron-skin thickness of ^{208}Pb [17,18] as well as the density dependence of the symmetry energy.

Of specific interest in this paper is the emergence and evolution of isoscalar monopole strength along the calcium isotopes. There are several reasons for undertaking such a study. First, the compressibility of neutron-rich matter is sensitive to both the incompressibility coefficient of symmetric nuclear matter and the density dependence of the symmetry

*jpiekarewicz@fsu.edu

energy [19]. Particularly interesting is to examine this sensitivity along an isotopic chain having several stable isotopes, such as calcium and tin. Note that although a decade has already passed since the "fluffiness" of tin was first identified [20–22], a theoretical explanation continues to elude us [23–36]. That is, theoretical models that account for giant monopole resonance (GMR) energies in ^{90}Zr, ^{144}Sm, and ^{208}Pb, overestimate the GMR energies in all stable tin— and cadmium ($Z=48$) [37]—isotopes. The imminent report of the GMR energy of the unstable ^{132}Sn nucleus may prove vital in elucidating the softness of tin [38]. In turn, an exploration of the evolution of the GMR energies along the isotopic chain in calcium above and beyond the already measured ^{40}Ca and ^{48}Ca isotopes [39–41] may be highly illuminating. This is particularly relevant given that existing experimental data seem to suggest an increase in the GMR energies with increasing mass, a fact that is difficult to reconcile with theoretical expectations [41]. Second, theoretical and computational advances have evolved to such an extent that *ab initio* calculations in the calcium region are now possible. *Ab initio* calculations now exist that can predict the electric dipole polarizability as well as the charge and weak form factors of both ^{40}Ca and ^{48}Ca [42]. Indeed, a primary motivation for the calcium radius experiment ("CREX") at Jefferson Lab is to bridge *ab initio* approaches with nuclear density functional theory [43]. Finally, extending GMR calculations beyond ^{48}Ca highlights the role of the continuum in the emergence of low-energy monopole strength. One expects that transitions out of the weakly bound pf neutron orbitals will result in the development of a soft monopole mode.

Although the compressibility of neutron-rich matter is primarily sensitive to the incompressibility coefficient of symmetric nuclear matter, a sensitivity to the symmetry energy develops in heavy nuclei with a significant neutron excess. Unfortunately, this sensitivity is often hindered by the relatively small neutron excess of the stable nuclei investigated up to date; note that the contribution from the symmetry energy scales as the *square* of the neutron-proton asymmetry $\alpha \equiv (N-Z)/A$ [19]. Hence, measuring the distribution of isoscalar monopole strength in unstable nuclei with a large neutron excess is highly appealing. Despite the relatively modest value of $\alpha_{68}=0.18$ (and $\alpha_{68}^2=0.03$) the measurement of the isoscalar monopole response of ^{68}Ni by Vandebrouck and collaborators represents an important first step in the right direction [44]. Although this pioneering experiment established the great potential of inelastic α scattering in inverse kinematics to probe the distribution of isoscalar monopole strength in unstable neutron-rich nuclei, a controversy ensued on the interpretation of the observed low-energy structure. Based on RPA predictions that used a discretized continuum, it was suggested that the observed low-energy strength consisted of individual peaks that were well separated from the main giant resonance [45,46]. Shortly after, Hamamoto and Sagawa concluded based on Skyrme–random phase approximation (RPA) calculations that did not rely on a discretization of the continuum, that the development of isoscalar monopole peaks in the low-energy region was very unlikely [47]; for an earlier account of the role of the continuum in the dynamics of the GMR in neutron-rich nuclei see Ref. [48]. Subsequently, relativistic RPA calculations confirmed that while a significant amount of low-energy strength in ^{68}Ni is indeed generated, such low-energy structure lacks any distinct features [49]. These findings suggest that a proper treatment of the continuum is critical. As is shown below, the continuum plays a fundamental role in the development of a soft monopole mode in all unstable neutron-rich calcium isotopes.

The paper has been organized as follows. In Sec. II a brief summary of the relativistic RPA formalism is presented highlighting the role of the continuum. In Sec. III I display both uncorrelated and RPA predictions for the distribution of isoscalar monopole strength along the isotopic chain in calcium for all even-even isotopes, from ^{40}Ca up to ^{60}Ca. In particular, special attention is paid to the role of the continuum in shaping the distribution of low-energy strength. Finally, a summary of the most important findings and suggestions for future work are provided in Sec. IV.

II. FORMALISM

The main goal of this section is to provide the technical material necessary to follow the discussion presented in Sec. III. The relativistic RPA formalism as implemented here has been reviewed extensively in earlier publications; see for example Refs. [33,49] and references contained therein. In particular, the critical role that the continuum plays on the emergence of low-energy isoscalar monopole strength has been extensively addressed in Ref. [49].

Isoscalar monopole response

In the relativistic mean-field (RMF) approach pioneered by Serot and Walecka [50,51], the basic constituents of the effective theory are protons and neutrons interacting via the exchange of the photon and various mesons of distinct Lorentz and isospin character. Besides the conventional Yukawa couplings of the mesons to the relevant nuclear currents, the model is supplemented by a host of nonlinear meson couplings that have been found essential to improve the standing of the model [52–54]. In the widely used mean-field approximation, the nucleons satisfy a Dirac equation in the presence of strong scalar and vector potentials that are the hallmark of the relativistic approach. In turn, the photon and the mesons satisfy classical Klein-Gordon equations with the relevant nuclear densities acting as a source term. As in most mean-field approaches, this close interdependence demands that the equations be solved self-consistently. In particular, the self-consistent procedure culminates with a few observables that fully characterize the mean-field ground state.

With these observables in place, one may proceed to compute the linear response of the mean-field ground state to an external perturbation. All dynamical information relevant to the excitation spectrum of the system is encoded in the *polarization propagator*, which is a function of both the energy and momentum transfer to the nucleus [55,56]. The first step in the calculation of the nuclear response is the construction of the *uncorrelated* (or mean-field) polarization propagator.

That is,

$$\Pi_{ab}(\mathbf{x},\mathbf{y};\omega) = \sum_{0<n<F} \overline{U}_n(\mathbf{x})\Gamma^a G_F(\mathbf{x},\mathbf{y};+\omega+E_n^{(+)})\Gamma^b U_n(\mathbf{y}) + \sum_{0<n<F} \overline{U}_n(\mathbf{y})\Gamma^b G_F(\mathbf{y},\mathbf{x};-\omega+E_n^{(+)})\Gamma^a U_n(\mathbf{x}), \quad (1)$$

where $E_n^{(+)}$ and $U_n(\mathbf{x})$ are single-particle energies and Dirac wave functions obtained from the self-consistent determination of the mean-field ground state, Γ^a contains information on the Lorentz and isospin structure of the operator responsible for the transition, and G_F is the "Feynman" propagator. Note that the sum is restricted to positive-energy states below the Fermi level. In turn, G_F may also be expressed as a sum over states by relying on its spectral decomposition:

$$G_F(\mathbf{x},\mathbf{y};\omega) = \sum_n \left(\frac{U_n(\mathbf{x})\overline{U}_n(\mathbf{y})}{\omega - E_n^{(+)} + i\eta} + \frac{V_n(\mathbf{x})\overline{V}_n(\mathbf{y})}{\omega + E_n^{(-)} - i\eta} \right), \quad (2)$$

where now $E_n^{(-)}$ and $V_n(\mathbf{x})$ represent single-particle energies and Dirac wave functions associated with the negative-energy part of the spectrum; recall that in the relativistic formalism the positive energy part of the spectrum by itself is not complete. However, note that now the spectral sum is unrestricted, as it involves bound and continuum states of positive and negative energy. In practice, one avoids carrying out this infinite sum by invoking a *nonspectral* representation of the Feynman propagator. This involves solving the following inhomogeneous differential equation for the Green's function in the mean-field approximation. That is,

$$(\omega\gamma^0 + i\boldsymbol{\gamma}\cdot\nabla - M - \Sigma_{\rm MF}(\mathbf{x}))G_F(\mathbf{x},\mathbf{y};\omega) = \delta(\mathbf{x}-\mathbf{y}), \quad (3)$$

where γ^0 and $\boldsymbol{\gamma} = (\gamma^1,\gamma^2,\gamma^3)$ are Dirac γ matrices, and $\Sigma_{\rm MF}$ is the *same exact* mean-field potential obtained from the self-consistent solution of the ground-state problem [33].

The uncorrelated mean-field polarization together with the residual interaction constitute the two main building blocks of the RPA polarization depicted in Fig. 1. By iterating the uncorrelated polarization to all orders, coherence is built through the mixing of all particle-hole excitations of the same spin and parity. If many particle-hole pairs get mixed, then the resulting RPA response displays strong collective behavior that manifests itself in the appearance of one "giant resonance" that often exhausts the classical sum rule [6]. If the residual interaction is attractive in the channel of interest (as in the case of the isoscalar monopole response) then the RPA distribution of strength is softened and enhanced relative to the uncorrelated response. If instead the residual interaction is repulsive (as in the case of the isovector dipole response) then the RPA response is hardened and quenched. For further details see Refs. [33,49].

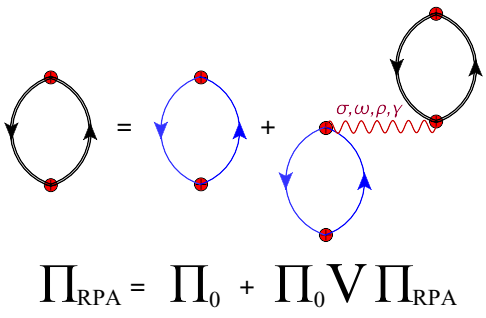

FIG. 1. Diagrammatic representation of the RPA equations. The ring diagram with the thick black lines represents the fully correlated RPA polarization while the one depicted with the thin blue lines is the uncorrelated mean-field polarization. The residual interaction denoted with the red wavy line must be identical to the one used to generate the mean-field ground state.

Given that the distribution of isoscalar monopole strength is the main focus of this paper, a brief description is now given on how to extract the response from the RPA polarization. To excite the appropriate $J^\pi = 0^+, T = 0$ channel, it is sufficient to use for the transition operator given in Eq. (1) the timelike component of the Dirac γ matrices, namely, $\Gamma^a = \Gamma^b = \gamma^0$. That is,

$$S(q,\omega;E0) = -\frac{1}{\pi}\mathrm{Im}\big(\Pi_{00}^{\rm RPA}(\mathbf{q},\mathbf{q};\omega)\big). \quad (4)$$

The above expression is still a function of both the energy and momentum transfer to the nucleus. In particular, "peaks" in the energy transfer are associated to the nuclear excitations and the area under the peaks are proportional to the transition form factor at the given momentum transfer. Since inelastic α scattering at forward angles is the experimental method of choice in isolating the isoscalar monopole strength from the overall cross section, $S(q,\omega;E0)$ is evaluated in the long wavelength limit. That is,

$$R(\omega;E0) = \lim_{q\to 0}\left(\frac{36}{q^4}\right) S(q,\omega;E0). \quad (5)$$

Often one is interested in computing moments of the strength distribution to extract centroid energies of the GMR. The moments of the distribution are defined as suitable energy weighted sums:

$$m_n(E0) \equiv \int_0^\infty \omega^n R(\omega;E0)\, d\omega. \quad (6)$$

Here special attention is paid to the energy weighted m_1, energy unweighted m_0, and inverse energy weighted m_{-1} sums [6].

A few comments that highlight the power of the nonspectral approach are in order. First, concerning the uncorrelated mean-field polarization depicted by the thin blue "bubble" in Fig. 1, the nonspectral framework adopted here is immune to most of the features that hinder the spectral approach, such as an energy cutoff and the discretization of the continuum. Indeed, some of these artifacts were responsible for the faulty interpretation of the structure of the low-energy monopole strength observed in ^{68}Ni [44]. Second, besides avoiding any reliance on artificial cutoffs and truncations, the nonspectral approach has the added benefit that both the positive- and negative-energy continua are treated exactly. Finally, in the context of the RPA response, it is important to underscore that in the interest of consistency, both the mean-field potential $\Sigma_{\rm MF}$ appearing in Eq. (3) as well

TABLE I. Parameter sets for the three models adopted in the text. All meson masses (m_s, m_v, and m_ρ) as well as κ are given in MeV. The nucleon mass has been fixed in all models at $M = 939$ MeV. See Ref. [71] for a definition of the model parameters.

Model	m_s	m_v	m_ρ	g_s^2	g_v^2	g_ρ^2	κ	λ	ζ	Λ_v
NL3	508.194	782.501	763.000	104.3871	165.5854	79.6000	3.8599	−0.015 905	0.000 000	0.000 000
FSUGold	491.500	782.500	763.000	112.1996	204.5469	138.4701	1.4203	+0.023 762	0.060 000	0.030 000
FSUGarnet	496.939	782.500	763.000	110.3492	187.6947	192.9274	3.2602	−0.003 551	0.023 500	0.043 377

as the residual particle hole interaction V depicted by the red wavy line in Fig. 1 must be fully consistent with the interaction used to generate the mean-field ground state. It is only in this manner that one can guarantee both the conservation of the vector current and the decoupling of the center-of-mass motion from the physical response [57–59].

I close this section by briefly addressing the emergence of low-energy strength in neutron-rich nuclei and its connections to fundamental parameters of the equation of state (EOS). Evidence of a soft dipole mode in exotic nuclei has generated considerable excitement as both a novel mode of excitation and as a possible constraint on the EOS [60–66]. One of the goals of the present study is to investigate how the distribution of isoscalar monopole strength in the calcium isotopes—particularly the appearance of a soft monopole mode—scales with mass number. To quantify the sensitivity of the bulk parameters of infinite nuclear matter to the isoscalar monopole response, the energy per particle of asymmetric nuclear matter at zero temperature is introduced:

$$E/A(\rho,\alpha) - M \equiv \mathcal{E}(\rho,\alpha) = \mathcal{E}_{\rm SNM}(\rho) + \alpha^2 \mathcal{S}(\rho) + \mathcal{O}(\alpha^4), \tag{7}$$

where $\rho = \rho_n + \rho_p$ is the nuclear density, $\mathcal{E}_{\rm SNM}$ is the energy per particle of symmetric nuclear matter, $\mathcal{S}$ is the symmetry energy, and α is the neutron-proton asymmetry. Now expanding the energy per particle around saturation density (ρ_0) one obtains

$$\begin{aligned}\mathcal{E}(\rho,\alpha) = &\left(\varepsilon_0 + \tfrac{1}{2}K_0 x^2 + \tfrac{1}{6}Q_0 x^3 + \cdots\right) \\ &+ \alpha^2\left(J + Lx + \tfrac{1}{2}K_{\rm sym}x^2 + \tfrac{1}{6}Q_{\rm sym}x^3 + \cdots\right) \\ &+ \mathcal{O}(\alpha^4),\end{aligned} \tag{8}$$

where $x = (\rho - \rho_0)/3\rho_0$ quantifies the deviation of the density from its value at saturation—and ε_0, K_0, and Q_0 denote the binding energy per nucleon, curvature (i.e., incompressibility), and skewness parameter of symmetric nuclear matter. In turn, J, $K_{\rm sym}$, and $Q_{\rm sym}$ represent the corresponding quantities for the symmetry energy. However, unlike symmetric nuclear matter which saturates, the symmetry pressure—or equivalently the slope of the symmetry energy L—does not vanish. In particular, L induces changes in the saturation density and incompressibility coefficient of *asymmetric neutron-rich matter* [19] that are given by

$$\rho_0(\alpha) = \rho_0 + \rho_\tau \alpha^2; \quad \text{with} \quad \rho_\tau \equiv -3\rho_0 \frac{L}{K_0}, \tag{9a}$$

$$K_0(\alpha) = K_0 + K_\tau \alpha^2; \quad \text{with} \quad K_\tau \equiv K_{\rm sym} - 6L - \frac{Q_0}{K_0}L. \tag{9b}$$

The above expression for K_τ suggests that measurements of the isotopic dependence of the giant monopole resonance in exotic nuclei with a very large neutron excess—such as the calcium isotopes—may place important constraints on the density dependence of the symmetry energy [20,23]. Important first steps along this direction have been already taken by Garg and collaborators [21,22,37].

III. RESULTS

I start this section by computing the distribution of isoscalar monopole strength for three relativistic mean-field models: (a) NL3 [67,68], FSUGold [69], and FSUGarnet [70]. Among these three, FSUGarnet is a recently calibrated parametrization that has been fitted to the ground-state properties of magic and semimagic nuclei, a few giant monopole energies, and well established properties of neutron stars [71]. In particular, FSUGarnet predicts that the isotopic chain in oxygen can be made to terminate at ^{24}O, as it has been observed experimentally [3]. The parameters for the three relativistic models adopted in this work are listed in Table I in terms of the Lagrangian density defined in Ref. [71].

Using the model parameters listed in Table I, one can then proceed to make predictions for a variety of bulk properties of infinite nuclear matter as defined in Eqs. (8) and (9). This set of bulk properties is displayed in Table II alongside quantities denoted as K_{40}, K_{48}, and K_{60} that represent the incompressibility coefficient of asymmetric matter having

TABLE II. Bulk parameters characterizing the behavior of infinite nuclear matter at saturation density as defined in Eqs. (8) and (9); M^* is the (Dirac) effective nucleon mass at saturation density. Here K_{40}, K_{48}, and K_{60} represent the incompressibility coefficient of asymmetric matter having the same neutron excess as ^{40}Ca, ^{48}Ca, and ^{60}Ni, respectively. All quantities are given in MeV except for ρ_0 which is given in fm^{-3} and M^* which is given in units of the free nucleon mass.

Model	ρ_0	M^*/M	ε_0	K_0	Q_0	J	L	$K_{\rm sym}$	K_τ	K_{40}	K_{48}	K_{60}
NL3	0.148	0.595	−16.24	271.5	209.5	37.29	118.2	100.9	−699.4	271.5	252.1	193.8
FSUGold	0.148	0.610	−16.30	230.0	−522.7	32.59	60.5	−51.3	−276.9	230.0	222.3	199.3
FSUGarnet	0.153	0.578	−16.23	229.5	4.5	30.92	51.0	59.5	−247.3	229.5	222.7	202.1

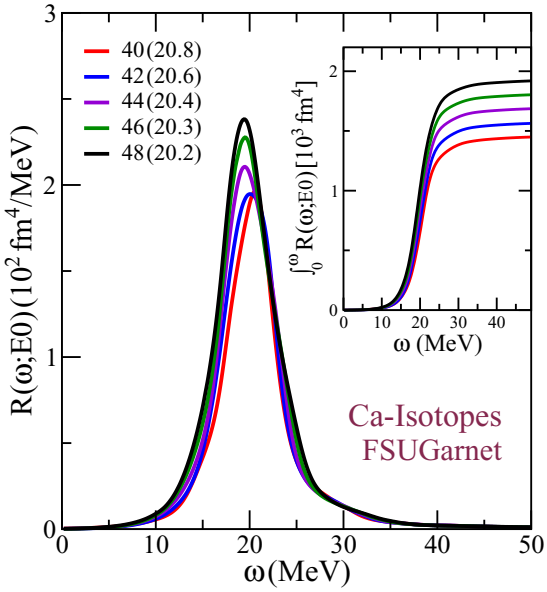

FIG. 2. Distribution of isoscalar monopole strength for the neutron-even calcium isotopes from ^{40}Ca up to ^{48}Ca as predicted by a relativistic RPA calculation using the FSUGarnet parametrization [70]. The numbers in parentheses represent the centroid energies defined as $E_{\rm cen} = m_1/m_0$. The inset displays the integrated strength, or "running sum," with the value at large excitation energy equal to the unweighted energy sum m_0.

the same neutron excess as ^{40}Ca($\alpha = 0$), ^{48}Ca($\alpha \simeq 0.167$), and ^{60}Ca($\alpha \simeq 0.333$), respectively. Although NL3 predicts an incompressibility coefficient K_0 that is considerably larger than the other two models, NL3 becomes the softest of the three models for infinite nuclear matter with a neutron excess equal to that of ^{60}Ca. This rapid softening of the incompressibility coefficient is attributed to NL3's stiff symmetry energy ($L \simeq 118$ MeV) which in turn is responsible for generating a large and negative value for K_τ. Hence, exploring the isotopic dependence of the ISGMR over an isotopic chain that includes exotic nuclei with a large neutron excess may become instrumental in constraining the density dependence of the symmetry energy.

The distribution of isoscalar monopole strength for all stable even-even calcium isotopes from ^{40}Ca to ^{48}Ca is displayed in Fig. 2 as predicted by the new FSUGarnet parametrization with the centroid energies m_1/m_0 shown in parentheses; see Eq. (6) and Table III. Although an enhancement of the response is evident as the $f^{7/2}$ neutron orbital is progressively being filled (see the inset in the figure) no appreciable softening is observed. This is somehow surprising given that as the $f^{7/2}$ orbital is being filled and the neutron-skin thickness steadily increases, the appearance of a soft monopole mode involving neutron-skin oscillations may have been natural. Yet, no low-energy monopole strength is detected. Values for the neutron-skin thickness of the calcium isotopes alongside other ground state properties are listed in Table IV. When available, experimental data for the binding energies [72] and charge radii [73,74] have also been included. The disagreement between theory and experiment typically amounts to a few percent. However, one should note that understanding the underlying physics behind the intriguing trend displayed by the charge radii, both in the stable [73] and unstable [74] isotopes, has been notoriously difficult; for a recent discussion of this topic see Refs. [75,76].

The predicted trend displayed in Fig. 2, however, is consistent with the expectation of a softening of the response with increasing mass number [6]. Hence, experimental evidence in favor of a centroid energy that is actually *lower* in ^{40}Ca than it is in ^{48}Ca [39,40] has baffled theoretical explanations; see Ref. [41] and references contained therein. As illustrated in Table III, this apparent anomaly remains unexplained in the present approach. Thus, mapping the experimental distribution of strength in the intermediate region of stable isotopes, from ^{42}Ca to ^{46}Ca, is highly encouraged as it may ultimately prove vital in solving the puzzle.

While no evidence of low-energy monopole strength was found in the stable calcium isotopes as the $1f^{7/2}$ neutron orbital was being filled, the situation changes dramatically with the occupation of the weakly bound $2p$ and $1f^{5/2}$ orbitals. In an effort to elucidate the nature of the low-energy monopole strength observed in the unstable calcium isotopes [see Fig. 5(a)] it is convenient to start by displaying in Fig. 3 the single-particle spectrum of ^{60}Ca as predicted by FSUGarnet; the arrows are used to indicate three prominent discrete proton excitations. Given that information about the mean-field excitation spectrum is fully contained in the uncorrelated response, the three discrete proton excitations in the $\omega \gtrsim 30$-MeV region are clearly discernible in Fig. 4(a) (the $d^{5/2}$ and $p^{1/2}$ excitations cannot be individually resolved in the figure). Besides these discrete proton excitations, two additional peaks are prominent in the 25–28-MeV region that cannot be inferred from the single-particle spectrum, as

TABLE III. Predictions for the centroid energies (all in MeV) for all stable even-even calcium isotopes obtained through two different moment ratios of the isoscalar monopole response displayed in Fig. 2 integrated up to a maximum value of $\omega_{\rm max} = 50$ MeV.

Isotope	NL3 [67,68]		FSUGold [69]		FSUGarnet [70]		Experiment [39,40]	
	m_1/m_0	$\sqrt{m_1/m_{-1}}$	m_1/m_0	$\sqrt{m_1/m_{-1}}$	m_1/m_0	$\sqrt{m_1/m_{-1}}$	m_1/m_0	$\sqrt{m_1/m_{-1}}$
^{40}Ca	22.29	21.52	21.53	20.76	20.81	20.09	19.2 ± 0.4	18.3 ± 0.4
^{42}Ca	22.04	21.28	21.39	20.74	20.64	20.02		
^{44}Ca	21.81	21.10	21.16	20.47	20.44	19.81		
^{46}Ca	21.56	20.89	21.00	20.34	20.31	19.69		
^{48}Ca	21.27	20.58	20.85	20.20	20.22	19.57	$19.88^{+0.14}_{-0.18}$	$19.04^{+0.11}_{-0.14}$

TABLE IV. Predictions for the binding energy per nucleon, charge radius, neutron radius, and neutron-skin thickness for all even-even $N \geqslant 20$ calcium isotopes. Binding energies are given in MeV and radii in fm. When available, experimental information is also provided.

Isotope	NL3 [67,68]				FSUGold [69]				FSUGarnet [70]				Expt. [72–74]	
	B/A	R_{ch}	R_n	R_{skin}	B/A	R_{ch}	R_n	R_{skin}	B/A	R_{ch}	R_n	R_{skin}	B/A	R_{ch}
^{40}Ca	8.543	3.456	3.329	−0.048	8.539	3.418	3.287	−0.051	8.531	3.425	3.293	−0.052	8.551	3.478
^{42}Ca	8.552	3.453	3.412	0.038	8.538	3.421	3.372	0.030	8.539	3.426	3.369	0.022	8.616	3.508
^{44}Ca	8.572	3.452	3.484	0.111	8.546	3.428	3.445	0.097	8.554	3.429	3.430	0.081	8.658	3.518
^{46}Ca	8.603	3.454	3.548	0.172	8.561	3.436	3.508	0.152	8.578	3.433	3.482	0.128	8.669	3.495
^{48}Ca	8.641	3.458	3.605	0.226	8.585	3.445	3.563	0.197	8.613	3.437	3.524	0.167	8.667	3.477
^{50}Ca	8.489	3.477	3.732	0.334	8.421	3.467	3.693	0.305	8.448	3.463	3.651	0.267	8.550	3.519
^{52}Ca	8.367	3.494	3.839	0.423	8.284	3.489	3.802	0.391	8.313	3.490	3.755	0.343	8.429	3.554
^{54}Ca	8.204	3.516	3.962	0.524	8.115	3.513	3.921	0.486	8.135	3.518	3.874	0.434	8.248	
^{56}Ca	8.038	3.553	4.035	0.559	7.937	3.548	3.982	0.512	7.923	3.559	3.943	0.461	8.040	
^{58}Ca	7.903	3.590	4.100	0.586	7.789	3.582	4.036	0.530	7.746	3.599	4.002	0.478	7.835	
^{60}Ca	7.793	3.627	4.159	0.608	7.667	3.616	4.084	0.543	7.600	3.638	4.051	0.488		

these involve transitions into the continuum. To illuminate the structure of these additional transitions, the two valence $2s^{1/2}$ and $1d^{3/2}$ proton orbitals are artificially removed, both having a binding energy of about 25 MeV (see Fig. 3). In particular, the curve denoted by porbs = 5 (red line) was obtained by removing the $2s^{1/2}$ orbital. The curve clearly shows how all the strength below ∼25 MeV practically disappears. This effect is further accentuated by removing both ($2s^{1/2}$ and $1d^{3/2}$) proton orbitals, resulting in the blue curve denoted by porbs = 4. Essentially, no monopole strength remains below 30 MeV.

If the role of the continuum is important in elucidating the character of the proton excitations, it becomes even more critical in understanding the nature of the neutron excitations—given that they all involve transitions into the continuum. Indeed, in Fig. 4(b) a significant amount of low-energy monopole strength is observed as a consequence of the excitation into the continuum of the weakly bound $2p$ and $1f^{5/2}$ states; see black line. As in the proton case, the role of these low-energy excitations is underscored by suppressing either three (red line) or four (blue line) transitions out of the valence $2p$-$1f$ orbitals. By doing so, essentially no monopole strength remains below $\omega \sim 18$ MeV. Moreover, it is interesting to note the two emerging discrete transitions out of the $1p$ states at $\omega \gtrsim 30$ MeV. The fact that these two Pauli-blocked transitions are completely suppressed from the complete calculation (black line) further validates the nonspectral treatment of the nuclear response. Before addressing the fully correlated RPA response, it is important to underscore the virtues of the nonspectral approach, especially in the context of weakly bound nuclei. The nonspectral Green's function approach adopted here allows for an exact treatment of the continuum without any reliance on artificial parameters. Indeed, introducing an energy cutoff or the discretization of the continuum is neither required nor admitted.

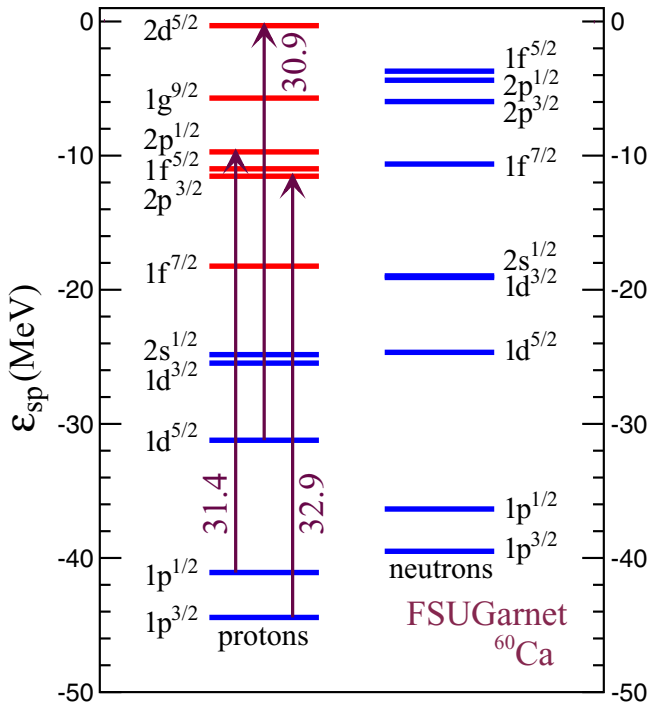

FIG. 3. Single-particle spectrum for ^{60}Ca as predicted by the relativistic FSUGarnet parametrization. The blue (red) lines denote occupied (empty) orbitals and the arrows indicate discrete transitions into bound states.

In Fig. 1 the diagrammatic representation of the RPA equations indicates how the correlated RPA response (solid black line) is obtained from the mean-field response (thin blue line) and the residual particle-hole interaction (wavy red line). Given that the RPA equations involve an iterative procedure to all orders, the singularity structure of the polarization is often changed dramatically. In the particular case of an attractive residual interaction, mixing a large number of particle-hole excitations results in the development of a single collective peak that exhausts most of the energy weighted sum [6], as is clearly evident in Fig. 2. However, for the unstable neutron-rich isotopes a significant amount of low-energy strength is expected to emerge as the result of transitions from weakly bound states into the continuum. This notion is confirmed in Fig. 5(a) that displays the distribution of isoscalar monopole strength for all unstable even-even calcium isotopes from ^{50}Ca to ^{60}Ca; the single-peak response of ^{48}Ca is also shown for reference. As in the case of Fig. 2, a giant resonance peak in the ∼17−20-MeV region is noticeable. Yet, a significant

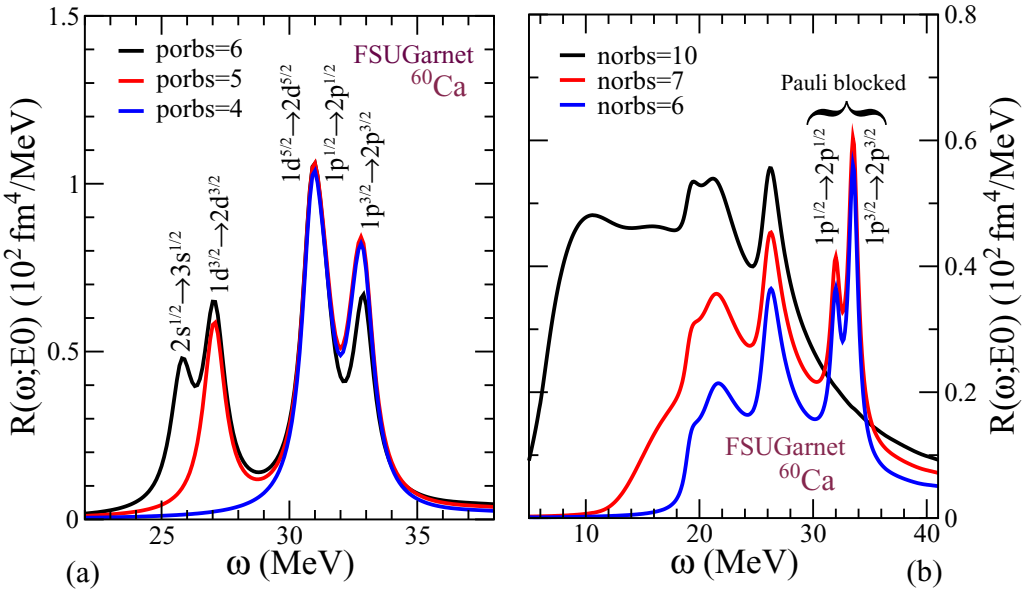

FIG. 4. Distribution of "uncorrelated" isoscalar monopole strength for ^{60}Ca as predicted by the FSUGarnet parametrization [70]. The left-hand panel (a) describes proton particle-hole excitations while the right-hand panel (b) depicts the corresponding neutron excitations. Transitions into bound states are easily identified both in this figure as well as in Fig. 3. See text for further details.

amount of low-energy monopole strength that progressively increases with mass number is also clearly evident. This can be quantified by plotting the running sum in the inset of Fig. 5(a). In contrast to the corresponding inset displayed in Fig. 2, a considerable amount of low-energy strength appears below 10 MeV. By somehow artificially dividing the giant-monopole region from the low-energy "pygmy" region at an excitation energy of $\omega = 11.5$ MeV, I display in Fig. 5(b) both the pygmy and giant contributions to the total unweighted energy sum m_0 as predicted by the FSUGold and FSUGarnet parametrizations. The figure clearly indicates the important contribution from the low-energy region to the overall m_0 moment. As expected, the pygmy contribution can be correspondingly enhanced or quenched by computing the inverse energy weighted sum m_{-1} or energy weighted sum m_1 as shown in Figs. 6(a) and 6(b), respectively. In particular, I observe nearly equal contributions from the pygmy and giant regions to the overall m_{-1} moment for ^{54}Ca. Recall that the electric dipole polarizability, which is proportional to the m_{-1} moment of the isovector dipole response, was identified as a strong isovector indicator that

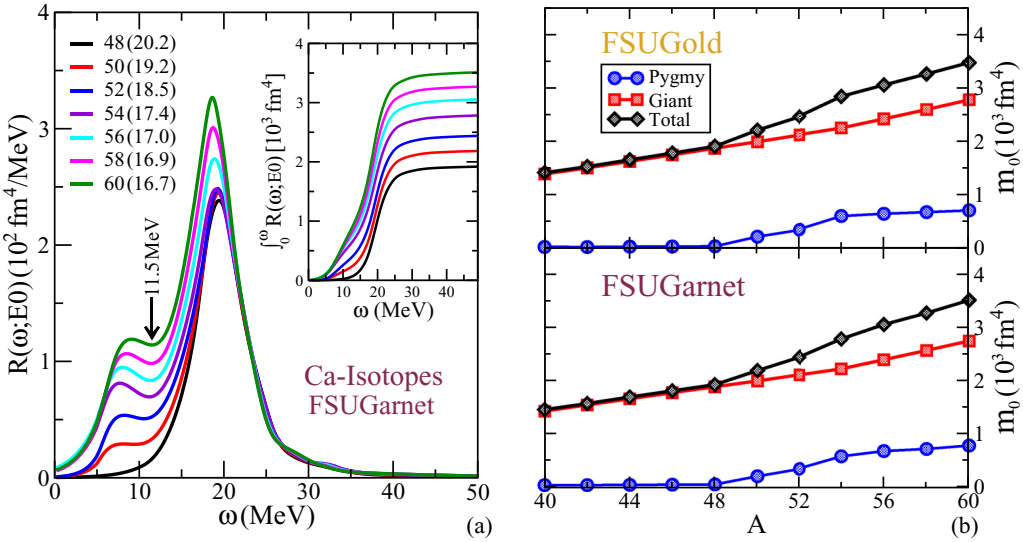

FIG. 5. (a) Distribution of isoscalar monopole strength for the neutron-even calcium isotopes from ^{48}Ca to ^{60}Ca as predicted by a relativistic RPA calculation using the FSUGarnet parametrization [70]. The numbers in parentheses represent the centroid energies defined as $E_{\rm cen} = m_1/m_0$. The inset displays the integrated strength, or "running sum," with the value at large excitation energy equal to the unweighted energy sum m_0. (b) Contribution from the low-energy ("Pygmy") and high-energy ("Giant") resonance region to the total unweighted energy sum m_0 for two relativistic parametrizations: FSUGold [69] and FSUGarnet.

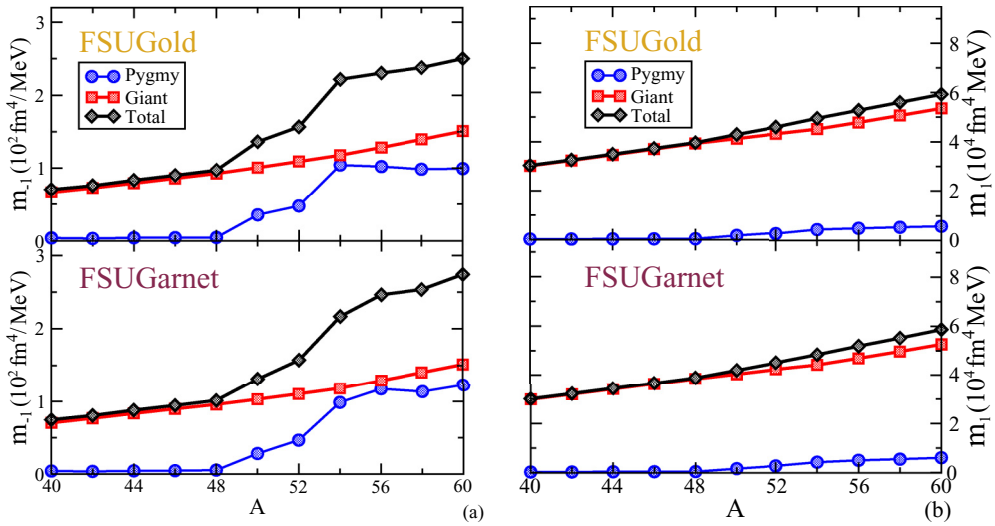

FIG. 6. Contribution from the low-energy ("Pygmy") and high-energy ("Giant") resonance region to the total (a) inverse energy weighted sum m_{-1} and (b) energy weighted sum m_1, as predicted by two relativistic parametrizations: FSUGold [69] and FSUGarnet [70].

is strongly correlated to both the neutron-skin thickness of neutron-rich nuclei and the slope of the symmetry energy [7]. As indicated in Table V and illustrated in Fig. 7, a correlation is also found between the neutron-skin thickness of the neutron-rich calcium isotopes and the total m_{-1} moment of the isoscalar monopole response. As already alluded to in earlier references, see for example Refs. [70] and [77], the softer the symmetry energy the earlier the neutron-drip line is reached. In essence, models with thin neutron skins predict weak binding energies for the valence neutron orbitals in neutron-rich nuclei. In the present case, FSUGarnet having the softest symmetry energy of the models employed here (see Table II) predicts the weakest binding for the valence $2p$-$1f^{5/2}$ neutron orbitals in the neutron-rich calcium isotopes and, as a consequence, the largest amount of low-energy monopole strength. In turn, NL3 having the stiffest symmetry energy displays the opposite trend: whereas it predicts the thickest neutron skins, its displays the least amount of low-energy monopole strength.

I conclude this section by displaying in Fig. 8 centroid energies for all three models considered in the text. Energies have been computed as both m_1/m_0 (black circles) and $\sqrt{m_1/m_{-1}}$ (red squares). Note that m_1/m_0 values also appear between parentheses in both Figs. 2 and 5(a). Besides these two choices, I include for reference centroid energies computed by assuming a Breit-Wigner (or Lorentzian) fit to only the giant monopole resonance (purple triangles). As the strength distribution for all stable calcium isotopes displayed in Fig. 2 is dominated by a single collective peak, fairly consistent results are obtained for all three choices. However, with the appearance of low-energy monopole strength in ^{50}Ca—and progressively more strength with increasing mass number—significant distortions to the simple Lorentzian shape emerge. This is reflected in a large dispersion among the three adopted definitions. Naturally, the Lorentzian fit to the GMR peak predicts the largest energy value, followed by m_1/m_0, and $\sqrt{m_1/m_{-1}}$ predicting the lowest value, because of the large enhancement in m_{-1}. Finally, although the last panel in the figure collects m_1/m_0 predictions from all three models, the notion of a centroid energy for a distribution of strength that is no longer dominated by a single collective peak loses most of its appeal.

TABLE V. Predictions for the neutron-skin thickness, and pygmy, giant, and total contributions to the inverse energy weighted sum m_{-1} for all even-even calcium isotopes from ^{50}Ca to ^{60}Ca. An excitation energy of $\omega = 11.5$ MeV was chosen to separate the pygmy from the giant resonance region; see Fig. 5(a). The neutron-skin thickness is given in fm and the m_{-1} values in fm^4/MeV.

Isotope	NL3 [67,68]				FSUGold [69]				FSUGarnet [70]			
	$R_{\rm skin}$	Pygmy	Giant	Total	$R_{\rm skin}$	Pygmy	Giant	Total	$R_{\rm skin}$	Pygmy	Giant	Total
^{50}Ca	0.334	23.78	96.55	120.33	0.305	35.50	100.61	136.11	0.267	28.27	102.99	131.26
^{52}Ca	0.423	36.30	105.06	141.36	0.391	47.66	109.01	156.67	0.343	46.76	110.45	157.21
^{54}Ca	0.524	75.42	114.24	189.66	0.486	104.15	117.62	221.77	0.434	98.61	118.15	216.75
^{56}Ca	0.559	83.30	126.32	209.62	0.512	102.10	128.28	230.38	0.461	117.39	129.09	246.48
^{58}Ca	0.586	68.16	138.88	207.05	0.530	98.52	139.36	237.88	0.478	113.47	140.13	253.60
^{60}Ca	0.608	76.73	152.31	229.04	0.543	99.29	150.83	250.12	0.488	122.86	151.37	274.22

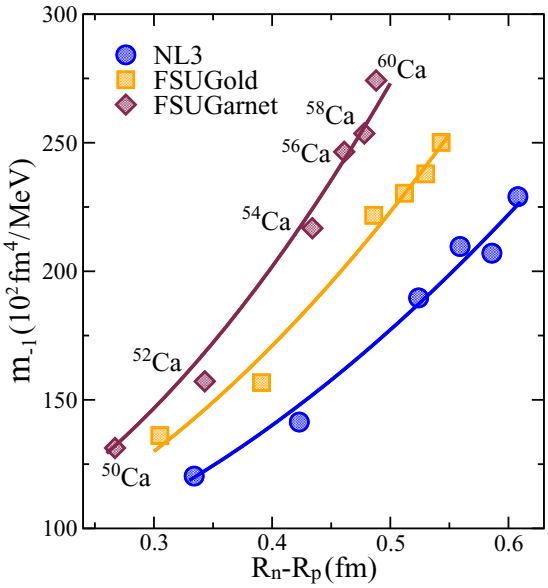

FIG. 7. Total (pygmy plus giant) inverse energy weighted sum as a function of the corresponding neutron-skin thickness for all even-even calcium isotopes from ^{50}Ca to ^{60}Ca. Predictions are displayed from all three relativistic models used in the text.

IV. CONCLUSIONS

The fascinating dynamics of exotic nuclei has lead to a paradigm shift in nuclear structure. *"How does subatomic matter organize itself and what phenomena emerge?"* and *"What combinations of neutrons and protons can form a bound atomic nucleus?"* are only a few of the most interesting questions energizing nuclear physics today. The main goal of this contribution was to explore the nature of the isoscalar monopole response in exotic calcium isotopes with extreme combinations of neutrons and protons.

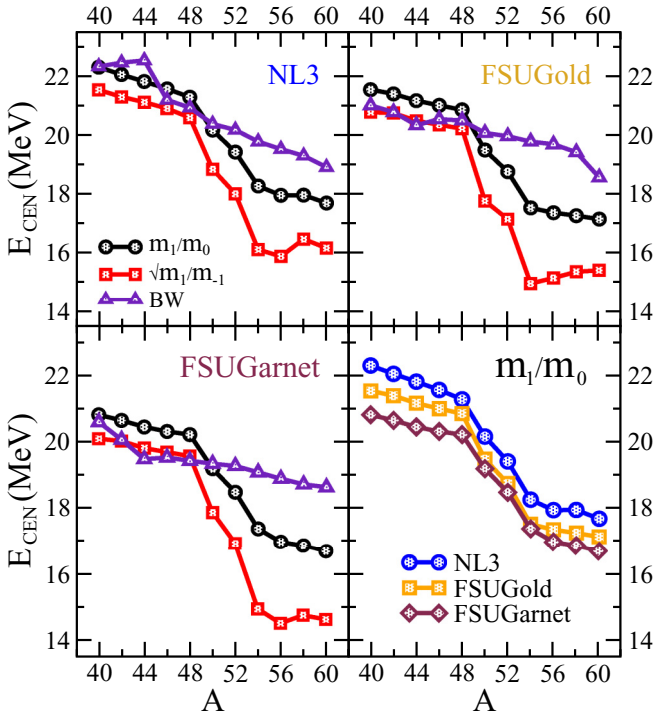

FIG. 8. Centroid monopole energies predicted by all three relativistic models NL3, FSUGold, and FSUGarnet for all even-even calcium isotopes from ^{40}Ca to ^{60}Ca. The various definitions adopted for the centroid energy have been discussed in the text.

At the most basic level, one would like to understand the scaling of the giant monopole resonance with increasing mass number, as it encodes information on the incompressibility of neutron-rich matter which, in turn, is sensitive to both the incompressibility coefficient of symmetric nuclear matter and the density dependence of the symmetry energy. Perhaps the biggest challenge in uncovering the sensitivity of the monopole resonance to the symmetry energy stems from the fact that its contribution scales as the square of the neutron-proton asymmetry. Thus, one most probe the dynamics of exotic nuclei far away from the valley of stability where the neutron-proton asymmetry is large. Important first steps along this direction have been taken along the isotopic chains in tin and cadmium. However, given that these measurements have been limited so far to stable isotopes, the neutron excess, although appreciable, is not yet sufficiently large. Yet, one is confident that in the new era of rare isotope facilities experimental studies of this kind will be extended well beyond stability.

An important motivation behind the current work was to confront the experimental observation that the distribution of isoscalar monopole strength in ^{40}Ca appears softer than in ^{48}Ca, in stark contrast with theoretical expectations. To do so, three relativistic mean-field models have been used that are known to provide a good description of ground-state properties throughout the nuclear chart. The disagreement with the experimental trend was confirmed for all three models considered here. Indeed, in examining the distribution of monopole strength in all stable even-even isotopes from ^{40}Ca to ^{48}Ca, a gradual, albeit small, softening of the monopole response with increasing mass number was found. This in spite of that one of the models adopted here ("FSUGarnet") was fitted to GMR energies of several magic and semimagic nuclei. Hence, measurements of the isoscalar monopole response of other stable calcium isotopes is strongly encouraged as it may play a vital role in resolving this discrepancy.

Yet the central goal of the present work was to study the emergence, evolution, and origin of low-energy monopole strength as a function of neutron excess. Somehow surprising, no evidence was found of a soft monopole mode in the stable calcium isotopes despite a steady increase in the thickness of the neutron skin. However, the situation changed dramatically with the occupation of the weakly bound neutron orbitals. Indeed, starting with ^{50}Ca and ending with ^{60}Ca, a well developed soft monopole mode of progressively increasing strength was clearly identified. The origin of the low-energy monopole strength was attributed to neutron excitations from the weakly bound orbitals into the continuum. As such, the RPA formalism employed here, based on a nonspectral approach that treats the continuum on the same footing as the bound states, is particularly advantageous. One should note that pairing correlations have been ignored throughout the paper. In the particular case of tin, it appears that pairing correlations do not provide the answer to the question of *why*

is tin so soft? However, unlike tin where the softening has only been observed in the well-bound stable isotopes, the situation in calcium may be different because the emergence of low-energy strength was evident along the weakly bound unstable isotopes. Thus, examining the impact (if any) of pairing correlations my be worthwhile.

Due to the prominent role played by the weakly bound neutron orbitals in generating low-energy monopole strength, a correlation to the density dependence of the symmetry energy was uncovered. This was motivated by the realization that models with a soft symmetry energy reach the neutron-drip line before their stiffer counterparts. In turn, this was reflected in the fact that the $2p$-$1f^{5/2}$ neutron orbitals are more weakly bound in FSUGarnet (the softest of the models employed in this work) than in NL3 (the model with the stiffest symmetry energy). As a result, FSUGarnet predicted a larger amount of low-energy monopole strength than NL3. On the other hand, models with a stiff symmetry energy generate thicker neutron skins. Hence, the following inverse correlation was proposed: the thinner the neutron skin, the larger the m_{-1} moment of the monopole distribution. Given that the isoscalar monopole response of the unstable ^{68}Ni isotope has already been measured in a pioneer experiment using inelastic α scattering in inverse kinematics, one is confident that such techniques may also be used to explore the monopole response of the exotic calcium isotopes. Such experiments will provide critical insights into the role of the continuum in understanding the physics of weakly bound systems and on the development of novel modes of excitation in exotic nuclei.

ACKNOWLEDGMENTS

The author wishes to express his gratitude to Professor U. Garg for many stimulating conversations. This material was based upon work supported by the US Department of Energy Office of Science, Office of Nuclear Physics under Award No. DE-FG02-92ER40750.

[1] *Reaching for the Horizon: The 2015 Long Range Plan for Nuclear Science*, https://science.energy.gov/~/media/np/nsac/pdf/2015LRP/2015_LRPNS_091815.pdf.
[2] *Perspectives in Nuclear Physics: NuPECC 2017 Long Range Plan for Nuclear Science*, http://www.nupecc.org/lrp2016/Documents/lrp2017.pdf.
[3] M. Thoennessen, Rep. Prog. Phys. **67**, 1187 (2004).
[4] R. Utama and J. Piekarewicz, Phys. Rev. C **96**, 044308 (2017).
[5] N. Paar, D. Vretenar, E. Khan, and G. Colò, Rep. Prog. Phys. **70**, 691 (2007).
[6] M. N. Harakeh and A. van der Woude, *Giant Resonances-fundamental High-frequency Modes of Nuclear Excitation* (Clarendon, Oxford, 2001).
[7] P.-G. Reinhard and W. Nazarewicz, Phys. Rev. C **81**, 051303 (2010).
[8] J. Piekarewicz, Phys. Rev. C **83**, 034319 (2011).
[9] J. Piekarewicz, B. K. Agrawal, G. Colò, W. Nazarewicz, N. Paar, P.-G. Reinhard, X. Roca-Maza, and D. Vretenar, Phys. Rev. C **85**, 041302(R) (2012).
[10] X. Roca-Maza, M. Brenna, G. Colò, M. Centelles, X. Viñas, B. K. Agrawal, N. Paar, D. Vretenar, and J. Piekarewicz, Phys. Rev. C **88**, 024316 (2013).
[11] A. Tamii *et al.*, Phys. Rev. Lett. **107**, 062502 (2011).
[12] I. Poltoratska, P. von Neumann-Cosel, A. Tamii, T. Adachi, C. Bertulani *et al.*, Phys. Rev. C **85**, 041304 (2012).
[13] T. Hashimoto *et al.*, Phys. Rev. C **92**, 031305(R) (2015).
[14] J. Birkhan *et al.*, Phys. Rev. Lett. **118**, 252501 (2017).
[15] O. Wieland *et al.*, Phys. Rev. Lett. **102**, 092502 (2009).
[16] D. Rossi, P. Adrich, F. Aksouh, H. Alvarez-Pol, T. Aumann *et al.*, Phys. Rev. Lett. **111**, 242503 (2013).
[17] S. Abrahamyan, Z. Ahmed, H. Albataineh, K. Aniol, D. S. Armstrong *et al.*, Phys. Rev. Lett. **108**, 112502 (2012).
[18] C. J. Horowitz, Z. Ahmed, C. M. Jen, A. Rakhman, P. A. Souder *et al.*, Phys. Rev. C **85**, 032501 (2012).
[19] J. Piekarewicz and M. Centelles, Phys. Rev. C **79**, 054311 (2009).
[20] U. Garg *et al.*, Nucl. Phys. **A788**, 36 (2007).
[21] T. Li *et al.*, Phys. Rev. Lett. **99**, 162503 (2007).
[22] T. Li *et al.*, Phys. Rev. C **81**, 034309 (2010).
[23] J. Piekarewicz, Phys. Rev. C **76**, 031301(R) (2007).
[24] H. Sagawa, S. Yoshida, G.-M. Zeng, J.-Z. Gu, and X.-Z. Zhang, Phys. Rev. C **76**, 034327 (2007).
[25] V. Tselyaev, J. Speth, S. Krewald, E. Litvinova, S. Kamerdzhiev, N. Lyutorovich, A. Avdeenkov, and F. Grümmer, Phys. Rev. C **79**, 034309 (2009).
[26] J. Li, G. Colò, and J. Meng, Phys. Rev. C **78**, 064304 (2008).
[27] J. Piekarewicz, J. Phys. G **37**, 064038 (2010).
[28] E. Khan, Phys. Rev. C **80**, 011307 (2009).
[29] E. Khan, Phys. Rev. C **80**, 057302 (2009).
[30] E. Khan, J. Margueron, G. Colò, K. Hagino, and H. Sagawa, Phys. Rev. C **82**, 024322 (2010).
[31] L.-G. Cao, H. Sagawa, and G. Colò, Phys. Rev. C **86**, 054313 (2012).
[32] P. Veselý, J. Toivanen, B. G. Carlsson, J. Dobaczewski, N. Michel, and A. Pastore, Phys. Rev. C **86**, 024303 (2012).
[33] J. Piekarewicz, Eur. Phys. J. A **50**, 25 (2013).
[34] G. Colò, U. Garg, and H. Sagawa, Eur. Phys. J. A **50**, 26 (2014).
[35] W.-C. Chen, J. Piekarewicz, and M. Centelles, Phys. Rev. C **88**, 024319 (2013).
[36] W.-C. Chen, J. Piekarewicz, and A. Volya, Phys. Rev. C **89**, 014321 (2014).
[37] D. Patel, U. Garg, M. Fujiwara, H. Akimune, G. Berg *et al.*, Phys. Lett. B **718**, 447 (2012).
[38] U. Garg (private communication).
[39] D. H. Youngblood, Y.-W. Lui, and H. L. Clark, Phys. Rev. C **63**, 067301 (2001).
[40] Y.-W. Lui, D. H. Youngblood, S. Shlomo, X. Chen, Y. Tokimoto, Krishichayan, M. Anders, and J. Button, Phys. Rev. C **83**, 044327 (2011).
[41] M. R. Anders, S. Shlomo, T. Sil, D. H. Youngblood, Y.-W. Lui, and Krishichayan, Phys. Rev. C **87**, 024303 (2013).
[42] G. Hagen *et al.*, Nat. Phys. **12**, 186 (2016).
[43] J. Mammei *et al.*, *CREX: Parity-violating Measurement of the Weak-charge Distribution of* ^{48}Ca *to 0.02 fm Accuracy* (2013).

[44] M. Vandebrouck, J. Gibelin, E. Khan, N. Achouri, H. Baba *et al.*, Phys. Rev. Lett. **113**, 032504 (2014).
[45] L. Capelli, G. Colò, and J. Li, Phys. Rev. C **79**, 054329 (2009).
[46] E. Khan, N. Paar, and D. Vretenar, Phys. Rev. C **84**, 051301 (2011).
[47] I. Hamamoto and H. Sagawa, Phys. Rev. C **90**, 031302 (2014).
[48] I. Hamamoto, H. Sagawa, and X. Z. Zhang, Phys. Rev. C **56**, 3121 (1997).
[49] J. Piekarewicz, Phys. Rev. C **91**, 014303 (2015).
[50] J. D. Walecka, Ann. Phys. **83**, 491 (1974).
[51] B. D. Serot and J. D. Walecka, Adv. Nucl. Phys. **16**, 1 (1986).
[52] J. Boguta and A. R. Bodmer, Nucl. Phys. **A292**, 413 (1977).
[53] H. Mueller and B. D. Serot, Nucl. Phys. **A606**, 508 (1996).
[54] C. J. Horowitz and J. Piekarewicz, Phys. Rev. Lett. **86**, 5647 (2001).
[55] A. L. Fetter and J. D. Walecka, *Quantum Theory of Many Particle Systems* (McGraw-Hill, New York, 1971).
[56] W. H. Dickhoff and D. van Neck, *Many-Body Theory Exposed* (World Scientific, Singapore, 2005).
[57] D. Thouless, Nucl. Phys. **22**, 78 (1961).
[58] J. F. Dawson and R. J. Furnstahl, Phys. Rev. C **42**, 2009 (1990).
[59] P. Ring and P. Schuck, *The Nuclear Many-body Problem* (Springer, New York, 2004).
[60] N. Tsoneva, H. Lenske, and C. Stoyanov, Phys. Lett. B **586**, 213 (2004).
[61] J. Piekarewicz, Phys. Rev. C **73**, 044325 (2006).
[62] N. Tsoneva and H. Lenske, Phys. Rev. C **77**, 024321 (2008).
[63] A. Klimkiewicz *et al.* (LAND Collaboration), Phys. Rev. C **76**, 051603(R) (2007).
[64] A. Carbone, G. Colò, A. Bracco, L.-G. Cao, P. F. Bortignon, F. Camera, and O. Wieland, Phys. Rev. C **81**, 041301(R) (2010).
[65] P. Papakonstantinou, H. Hergert, V. Y. Ponomarev, and R. Roth, Phys. Rev. C **89**, 034306 (2014).
[66] D. Savran, T. Aumann, and A. Zilges, Prog. Part. Nucl. Phys. **70**, 210 (2013).
[67] G. A. Lalazissis, J. Konig, and P. Ring, Phys. Rev. C **55**, 540 (1997).
[68] G. A. Lalazissis, S. Raman, and P. Ring, At. Data Nucl. Data Tables **71**, 1 (1999).
[69] B. G. Todd-Rutel and J. Piekarewicz, Phys. Rev. Lett **95**, 122501 (2005).
[70] W.-C. Chen and J. Piekarewicz, Phys. Lett. B **748**, 284 (2015).
[71] W.-C. Chen and J. Piekarewicz, Phys. Rev. C **90**, 044305 (2014).
[72] W. J. Huang, G. Audi, M. Wang, F. G. Kondev, S. Naimi, and X. Xu, Chin. Phys. C **41**, 030002 (2017).
[73] I. Angeli and K. Marinova, At. Data Nucl. Data Tables **99**, 69 (2013).
[74] R. F. G. Ruiz *et al.*, Nat. Phys. **12**, 594 (2016).
[75] R. Utama, W.-C. Chen, and J. Piekarewicz, J. Phys. G **43**, 114002 (2016).
[76] P. G. Reinhard and W. Nazarewicz, Phys. Rev. C **95**, 064328 (2017).
[77] B. G. Todd and J. Piekarewicz, Phys. Rev. C **67**, 044317 (2003).